ACS OMEGA

Article

Cite This: ACS Omega 2019, 4, 21612−21619

http://pubs.acs.org/journal/acsodf

Self-Assembled Regenerated Silk Fibroin Microsphere-Embedded Fe_3O_4 Magnetic Nanoparticles for Immobilization of Zymolyase

Menglin Xiao and Shanshan Lv*

State Key Laboratory of Organic-Inorganic Composite Materials, Beijing University of Chemical Technology, 15 BeisanhuanDong Road, Chaoyang District, Beijing 100029, China

Supporting Information

ABSTRACT: Cytoplasm of *Saccharomyces cerevisiae* yeast cells contains a significant amount of desired intracellular products for both industrial utility and academic research. To recover intracellular compounds, it is necessary to break the yeast cells with high efficiency, which, under certain circumstances, requires the use of the lytic enzyme zymolyase to completely digest the cell walls. A promising strategy for zymolyase immobilization on silk fibroin (SF) was developed. SF/Fe_3O_4 magnetic microspheres (MMs) were constructed by solvent (ethanol)-induced self-assembly of SF surrounding Fe_3O_4 magnetic nanoparticles (MNs), which were synthesized by a coprecipitation method. Zymolyase was covalently bonded on the surface of the SF/Fe_3O_4 MMs by a photochemical cross-linking method to produce robust biocatalysts of zymolyase/SF/Fe_3O_4. The chemical, magnetic, and morphological properties of the MM supports and the immobilized zymolyase were investigated. Enzymolysis results demonstrated that the immobilized zymolyase showed good activity and stability for digesting yeast cell walls, and the biocatalyst can be readily recycled through convenient magnetic separation for reuse. At the optimum pH = 7.5, the immobilized zymolyase maintained 84% of the activity of the free zymolyase and retained 41% of its initial activity after four times of reuse. At unfavorable acidic pH = 4, the immobilized zymolyase retained 81% of its initial activity, while the free zymolyase showed no significant activity. Consequently, the SF/Fe_3O_4 MMs exhibit superior performance in terms of immobilizing enzymes, which have a good prospect in the biological application.

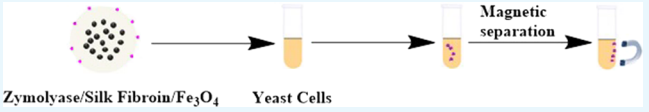

INTRODUCTION

Yeast *Saccharomyces cerevisiae* (*S. cerevisiae*) has a significant industrial utility. Because the cellular structure and functional organization of *S. cerevisiae* are similar to those of plant and animal cells, it is one of the most intensively studied unicellular eukaryotic model organisms in biological research.[1] Cytoplasm of *S. cerevisiae* is a rich source of bioproducts (such as proteins, polysaccharides, and so on) valuable in biotechnology and pharmacology, as well as in the food industry. Recovery of the intracellular products requires efficient disruption of the yeast cells. For example, thanks to its genetic tractability, short generation time, and easy cultivation, *S. cerevisiae* has been widely used for the expression of recombinant posttranslationally modified proteins. Many recombinant proteins expressed in *S. cerevisiae* remain intracellular and need to be released by disrupting the yeast cells.[2] However, *S. cerevisiae* has a relatively thick and rigid cell wall consisting of β-glucan, mannan, and glycoprotein, which is notoriously difficult to break.[3] Various methods have been reported, such as freeze/thawing, high-frequency focused and conventional (ultra)sonication, high-pressure homogenization, osmotic shock, bead milling, and chemical or enzymatic lysis.[2,4] For laboratory-scale cell disruption for intracellular protein recovery, the enzymatic and chemical lysis methods are commonly used. For enzymatic lysis, zymolyase accumulated from *Arthrobacter luteus* (*A. luteus*) culture is a mixture of lytic enzymes, including β-1,3-glucanase, mannose, and protease, and can readily degrade viable yeast cell walls at all growth stages under mild reaction conditions.[5]

However, practical applications of native zymolyase are seriously limited by its high sensitivity to environmental conditions, unsatisfactory operational and storage stability, low marginal lifetime, lack of (re)-purification, difficulties in recovery, and reusability.[6,7] Immobilization of enzymes on supports/carriers has been most commonly used to improve the efficiency of enzymes for industrial utilizations. The effect of immobilization depends upon the supports and immobilization procedure.[8−11] Particularly, iron oxide (Fe_3O_4) magnetic nanoparticles (MNs) have attracted a great deal of interest in enzyme immobilization as they provide a facile and effective separation of enzymes from the biocatalytic reaction mixture by use of external magnetic fields and thereby recovery of the enzymes for continual uses.[12] Generally, bare Fe_3O_4 MNs have a tendency to aggregate and are sensitive to oxidation and acidic conditions, which hinder their practical applications. Active groups on Fe_3O_4 MNs are limited, which results in incompetence of naked Fe_3O_4 MNs for direct attachment of enzymes. At this junction, functionalization on the surface of Fe_3O_4 MNs is a promising strategy. A range of natural

Received: October 19, 2019
Accepted: November 20, 2019
Published: December 5, 2019

DOI: 10.1021/acsomega.9b03491
ACS Omega 2019, 4, 21612−21619

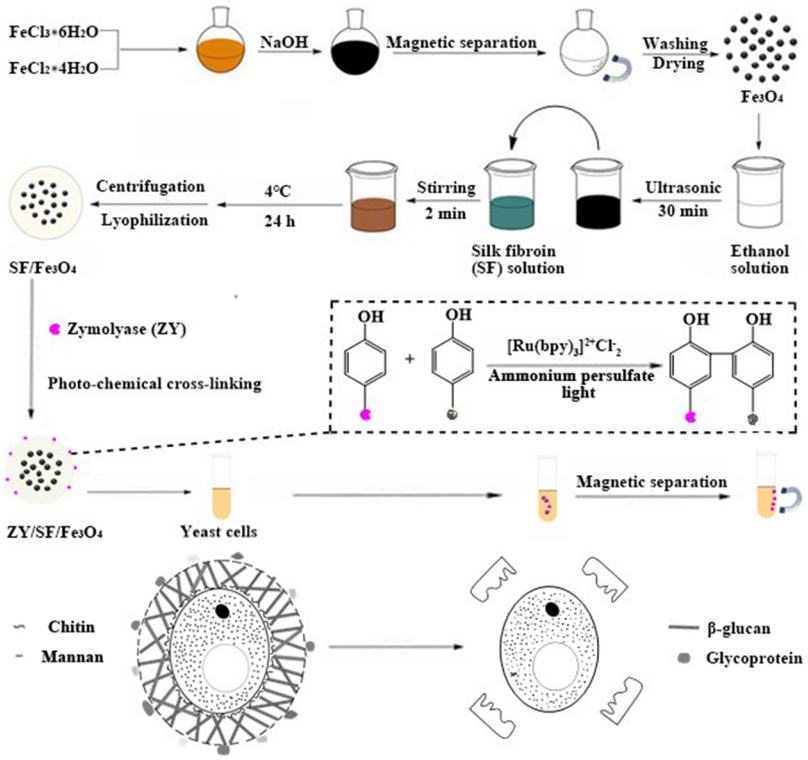

Figure 1. Schematic illustration of zymolyase immobilization on regenerated silk fibroin microspheres embedding Fe_3O_4 magnetic nanoparticles and the mechanism of zymolyase disrupting yeast cell walls.

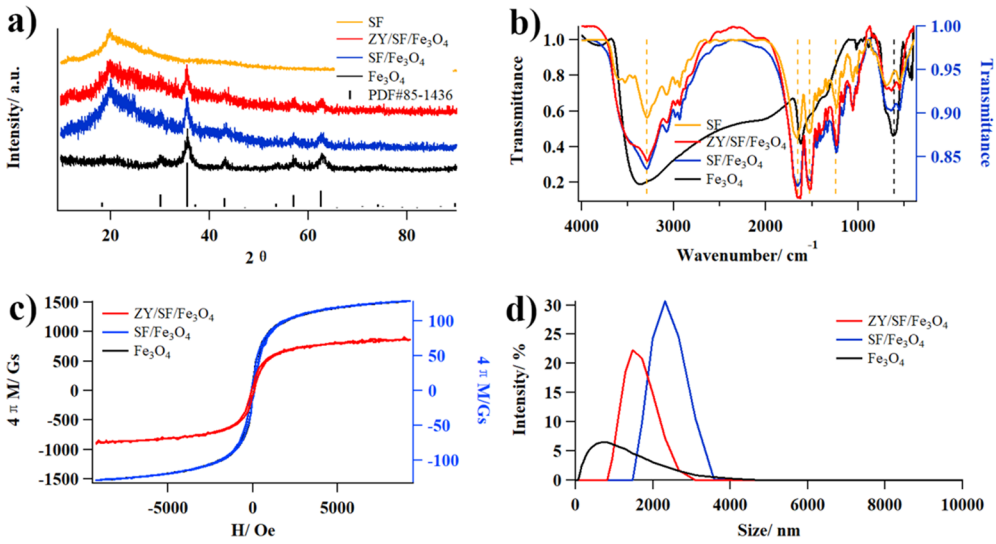

Figure 2. Chemical characterization of Fe_3O_4, SF/Fe_3O_4, and $ZY/SF/Fe_3O_4$. (a) XRD patterns. (b) FTIR spectra. (c) Magnetic hysteresis loops. (d) DLS curves.

polymers with various functional groups have been developed to modify Fe_3O_4 MNs.[13−17]

Silk fibroin (SF) derived from *Bombyx mori* is an abundant sustainable biopolymer with more than 480,000 tons per year produced all over the world. SF exhibits an impressive versatile processability and good ability to be functionalized.[18] Particularly, SF has been investigated in the field of enzyme immobilization.[19,20] In our previous studies, SF-based hydrogels were fabricated for immobilization of several industrially important enzymes; the immobilized enzymes displayed a wide-working pH range, as well as recyclability.[21−25] In addition, several methods have been developed to prepare SF-coated MNs.[26,27] For instance, Chen and co-workers fabricated Fe_2O_3/SF nanoparticles.[26] Huang and co-workers fabricated Fe_3O_4/SF nanoparticles with irregular structures.[27] Lu and co-workers fabricated core−shell Fe_3O_4/SF microspheres with controllable homogeneous size and water dispersibility by a one-step solvothermal process.[28] Tian et al. prepared Fe_3O_4/SF nanoparticles by a one-step potassium phosphate salting-out process.[29] These SF-based MNs of many pioneering works have been widely used in biomedical applications such as drug delivery and magnetic resonance imaging (MRI).[30] Despite the progress on SF/Fe_3O_4 magnetic materials, their application in enzyme immobilization and

DOI: 10.1021/acsomega.9b03491
ACS Omega 2019, 4, 21612−21619

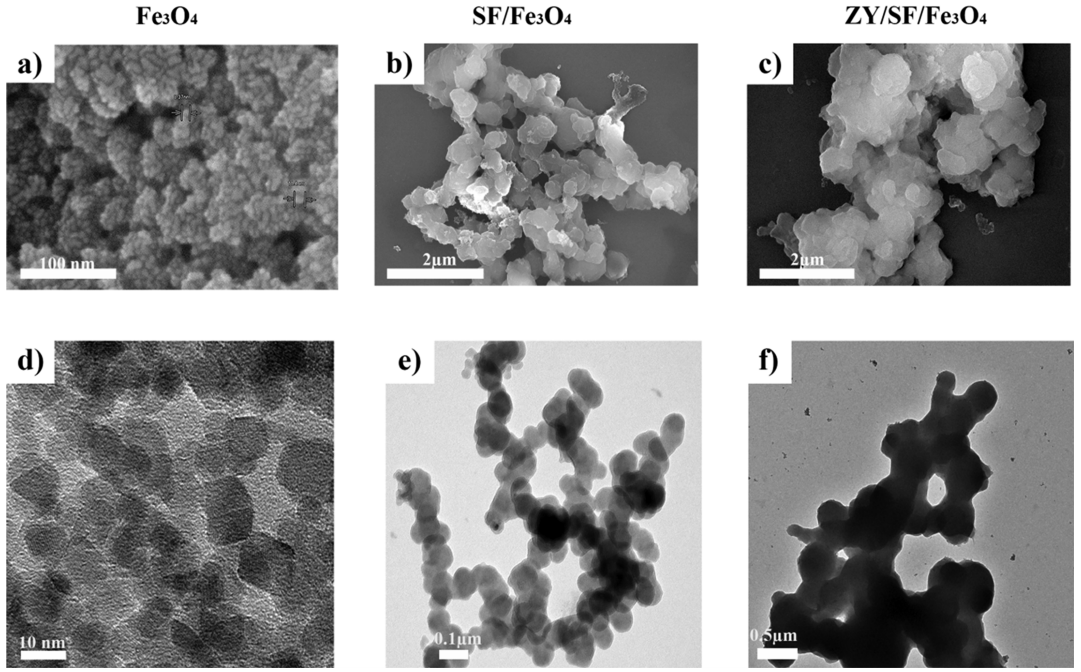

Figure 3. Morphological characterization of Fe_3O_4, SF/Fe_3O_4, and ZY/SF/Fe_3O_4. Representative (a–c) SEM images and (d–f) TEM images.

development of an efficient method to achieve high performances has a substantial demand.[31]

Herein, we aimed to explore the possibility of covalently immobilizing zymolyase on SF/Fe_3O_4 magnetic microspheres (ZY/SF/Fe_3O_4) for effectively disrupting *S. cerevisiae* yeast cells. The proposed process is schematically illustrated in Figure 1. First, Fe_3O_4 MNs were synthesized through coprecipitation of ferrous (Fe^{2+}) and ferric (Fe^{3+}) ions in a basic aqueous medium.[32,33] The obtained Fe_3O_4 MNs can be uniformly dispersed in ethanol and water. Then, through a controllable ethanol-induced interface self-assembly,[26,34] SF embedded the Fe_3O_4 MNs, forming SF/Fe_3O_4 MMs. Subsequently, the abundant tyrosine residues of SF were employed for immobilization of zymolyase through Ru(II)-mediated photochemical cross-linking reactions between the phenyl groups of SF and zymolyase, initiated by ammonium persulfate (APS). Thus, zymolyase was covalently bonded on the surface of the SF/Fe_3O_4 MMs, obtaining the ZY/SF/Fe_3O_4. It is of note that the SF not only served as a matrix for enzyme immobilization but also served as a protective layer for the Fe_3O_4 MNs. Owing to a large amount of serine residues (hydroxyl groups) in SF, SF stabilized the Fe_3O_4 MNs through electrostatic adsorption and hydrogen bonding interactions, preventing aggregation and avoiding corrosion or oxidation in subsequent reaction media. The resultant materials were examined by X-ray powder diffraction (XRD), Fourier transform infrared (FTIR) spectroscopy, dynamic light scattering (DLS), thermogravimetric analysis (TGA), vibrating sample magnetometers (VSM), transmission electron microscopy (TEM), and scanning electron microscopy (SEM) equipped with energy-dispersive spectrometer (EDS). The activity of the immobilized zymolyase on cell disruption was evaluated by enzymolysis assays via measurement of UV–vis spectroscopy. The cell disruption kinetics was also investigated.

RESULTS AND DISCUSSION

Crystalline Structure Analysis. The XRD patterns of Fe_3O_4, SF/Fe_3O_4, and ZY/SF/Fe_3O_4 (Figure 2a) exhibited the same diffraction peaks, which could be assigned to characteristic peaks of the standard Fe_3O_4 (PDF#85-1436) compiled by the International Center for Diffraction Data (ICDD). The peaks at 2θ values of 30.1, 35.4, 37.1, 43.1, 53.4, 57.0, and 62.6° were indexed as (220), (311), (222), (400), (422), (511), and (440) planes of the phase pure spinel structure of Fe_3O_4, respectively.[35] On one hand, the crystalline structure of Fe_3O_4 did not change after being embedded in SF/Fe_3O_4.[31] On the other hand, new peaks at 2θ = 20.2° ascribed to SF appeared in SF/Fe_3O_4 and ZY/SF/Fe_3O_4, indicating that SF was successfully coated on Fe_3O_4. Specifically, TGA results showed that the contents of Fe_3O_4 in SF/Fe_3O_4 and ZY/SF/Fe_3O_4 were 39.0 ± 1.1 and 46.3 ± 0.1%, respectively (Figure S1).

Chemical Composition. The FTIR spectra of Fe_3O_4, SF/Fe_3O_4, and ZY/SF/Fe_3O_4 are displayed in Figure 2b. The characteristic peak of Fe_3O_4 was at 605 cm^{-1}.[36] The characteristic peaks of SF were at 1650, 1525, and 1240 cm^{-1}, belonging to β-sheets, typical secondary structures of regenerated SF.[21] In the spectra of SF/Fe_3O_4 and ZY/SF/Fe_3O_4, both Fe_3O_4 and SF were observed, also indicating that SF was successfully coated on Fe_3O_4.[37] The chemical composition of SF/Fe_3O_4 and ZY/SF/Fe_3O_4 was further confirmed by EDS analysis (Figure S2), showing existence of the elements Fe, O, C, and N. The appearance of C and N signals observed in SF/Fe_3O_4 and ZY/SF/Fe_3O_4 may be originated from SF and the immobilized zymolyase, also indicating that SF was successfully coated onto the surface of Fe_3O_4. EDS mapping analysis also demonstrated homogeneous distribution of Fe and thereby Fe_3O_4 in SF/Fe_3O_4 and ZY/SF/Fe_3O_4.

Magnetic Properties. The magnetic hysteresis loops of Fe_3O_4, SF/Fe_3O_4, and ZY/SF/Fe_3O_4 exhibited low coercivity and small hysteresis (Figure 2c). The saturation magnetization

DOI: 10.1021/acsomega.9b03491
ACS Omega 2019, 4, 21612–21619

values (at H = 4000 Oe) of Fe_3O_4, SF/Fe_3O_4, and ZY/SF/Fe_3O_4 were 1180, 91.1, and 53.8 Gs, respectively, indicating that all of the samples possessed magnetic responsiveness.[31] The saturation magnetization decreased after SF coating and zymolyase immobilization. This phenomenon can be explained by the presence of SF layers around Fe_3O_4, as revealed by larger sizes of SF/Fe_3O_4 (~2157 nm) and ZY/SF/Fe_3O_4 (~1289 nm) than that of Fe_3O_4 (~479 nm). It is of note that hydrodynamic sizes determined by DLS (Figure 2d) might differ from particle sizes measured by other techniques such as TEM and SEM. Nevertheless, ZY/SF/Fe_3O_4 could be quickly separated from the reaction mixtures by magnets and rapidly redispersed when the magnetic field disappeared. The sensitive magnetic responsivity and redispersibility implied that ZY/SF/Fe_3O_4 possessed advantageous properties for magnetic manipulation as biocatalysts.

Morphology Analysis. The SEM images of Fe_3O_4, SF/Fe_3O_4, and ZY/SF/Fe_3O_4 are represented in Figure 3a−c, respectively. Fe_3O_4 displayed roughly spherical structures. SF/Fe_3O_4 was larger than Fe_3O_4, suggesting that the Fe_3O_4 MNs were embedded into the SF microsphere. Thanks to the distinct density contrast, TEM images might be easy to differentiate the samples. The TEM images of Fe_3O_4, SF/Fe_3O_4, and ZY/SF/Fe_3O_4 are depicted in Figure 3d−f, respectively. After self-assembly of SF on Fe_3O_4, SF/Fe_3O_4 MMs comprising Fe_3O_4 (black) and thin SF layers (gray) were observed. The images confirmed a uniform fine spherical shape of SF/Fe_3O_4 and ZY/SF/Fe_3O_4. ZY/SF/Fe_3O_4 was denser and larger than SF/Fe_3O_4. The TEM observation was consistent with those of SEM.

Immobilization Efficiency. The immobilization capacity and efficiency would be affected by many factors, including reaction time, pH, temperature, concentration of zymolyase, and activation of chemical bonds on both SF and zymolyase. In the present study, zymolyase was immobilized on the SF/Fe_3O_4 MMs via cross-linking of tyrosine residues into dityrosine adducts. The presence of tyrosine residues in both SF[25] and zymolyase were confirmed by amino acid analysis (Table 1). Following immobilization of zymolyase on SF/Fe_3O_4, the loading capacity was determined using the classical Bradford protein assay, showing an immobilization efficiency of almost 100% at a loading amount of 100 mg·g^{-1}. Furthermore, as the immobilization of zymolyase occurs via covalent bonds, no leaching of zymolyase was observed.

Table 1. Amino Acid Analysis of Zymolyase

amino acids	content (wt %)	amino acids	content (wt %)
$CySO_3H$	0.632	Met	0.831
Tau	0.031	Ile	2.772
Asp	9.687	Leu	5.171
Thr	5.961	Tyr	3.069
Ser	4.118	Phe	3.222
Glu	9.355	g-ABA	0.128
Gly	5.126	Thr-ol	0.776
Ala	6.057	Lys	2.616
Cys	1.445	NH_3	30.194
Val	5.210	Arg	3.600

Enzymatic Activity. During lysis of viable yeast cells, turbidity of the reaction mixture decreased with time and became approximately constant after 2 h. At 0.5 h intervals, the number of yeast cells was counted (Figure 4a). In the case of free zymolyase, as the enzyme concentration increased from 0.1 to 1.0 mg·mL^{-1}, no significant change in either reaction rate or product yield was observed (Figure S3a). As pH influenced the lytic activity considerably, the effect of pH on the free zymolyase was examined (Figure 4b). The optimum pH of the free zymolyase was pH = 7−8. High lytic activities were detected at pH = 9−10. However, only weak lytic activity was observed at pH = 6; almost no lytic activity was detected at pH ≤ 5. Compared with the free enzyme, the immobilized enzyme usually exhibited reduced activity.[12,22,38,39] Thus, a comparative investigation between the free and immobilized zymolyase was conducted in terms of pH in the range of 4−10. At pH = 7.5, the immobilized zymolyase maintained 84% of the activity of the free zymolyase. The immobilized zymolyase maintained a relatively high activity over 4−6. At pH = 4, the immobilized zymolyase retained 81% of its initial activity, which was higher than that of the free zymolyase. The tolerance to unfavorable acidic pH of zymolyase had been significantly enhanced after immobilization.

Kinetic Parameters. It should be noted that, in our previous studies on enzymes immobilized in SF-based hydrogels, deviation of the kinetic data from a first-order equation to an "S"-shaped curve was observed. The change in the kinetic properties of enzymes was mainly attributed to the mass transfer limitations.[22] In the present study, zymolyase immobilized on SF/Fe_3O_4 MMs showed higher activities than that on SF-based hydrogels under the same condition (Figure S3b), yet the enzymolysis data fit well with the first-order kinetic expression. To further understand the zymolyase activity, Michaelis−Menten kinetics of yeast cell disruption was measured at different initial substrate concentrations. The kinetic parameters for the free and immobilized zymolyase were calculated from the Lineweaver−Burk plots (Figure 4c). K_m values for the free and immobilized zymolyase were 1.0 × 10^5 and 1.4 × 10^4 cfu·mL^{-1}, respectively. K_{cat}/K_m for the free zymolyase was 0.44 L·g^{-1}·h^{-1}, whereas that of the immobilized zymolyase was 0.34 L·g^{-1}·h^{-1}. The slight decrease might be caused by a possible structural change and conformational hindrance of the active sites after immobilization of zymolyase on SF/Fe_3O_4.[12,38,39] Reusability of the immobilized zymolyase was also evaluated. ZY/SF/Fe_3O_4 could be magnetically separated, recovered, and retained 41% of its initial activity after four consecutive cycles (Figure 4d). This observation demonstrated an improved reusability of ZY/SF/Fe_3O_4, which was crucial and attractive for practical application in digesting yeast cell walls.

CONCLUSIONS

SF MM-embedded Fe_3O_4 MNs were prepared as effective magnetic carriers for enzyme immobilization. Zymolyase was used as a model enzyme and was successfully immobilized on SF/Fe_3O_4. The SF/Fe_3O_4 MMs exhibited high immobilization efficiency and a capacity reaching 100 mg·g^{-1}. Compared with the free zymolyase, the immobilized zymolyase exhibited good biocatalytic activity for disruption of *S. cerevisiae* cells in a wide range of pH. Moreover, the saturation magnetization value of ZY/SF/Fe_3O_4 was 53.8 Gs, which allowed reuse of the immobilized zymolyase by magnetic treatment. The results validated that the SF MMs are promising platforms for enzyme immobilization with high performance. Through the introduction of Fe_3O_4 MNs and immobilization of zymolyase, this study provides an effective strategy to further improve the performance of SF-based materials.

DOI: 10.1021/acsomega.9b03491
ACS Omega 2019, 4, 21612−21619

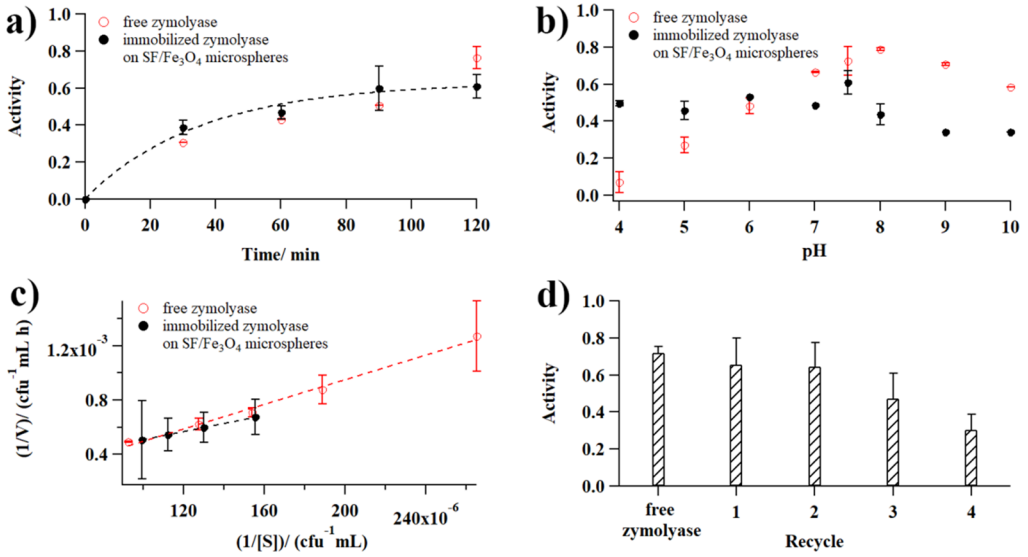

Figure 4. Enzymolysis assays on the free and immobilized zymolyase. (a) Time course of lysis of yeast cells. (b) Changes of lytic activities at different pH. (c) Lineweaver–Burk plots for the free and immobilized zymolyase. (d) Reusability of ZY/SF/Fe_3O_4.

EXPERIMENTAL SECTION

Materials. Zymolyase from *A. luteus* was purchased from Nacalai Tesque, Inc. (Japan). Sodium hydroxide (NaOH; 98%), ferrous chloride ($FeCl_2{\cdot}4H_2O$; 98%) and ferric chloride ($FeCl_3{\cdot}6H_2O$; 99%) were purchased from Macklin. Ammonium persulfate (APS) and tris(2,2′-bipyridyl)-dichlororuthenium(II) hexahydrate ($[Ru(bpy)_3]^{2+}Cl^-_2{\cdot}6H_2O$) were purchased from Sigma-Aldrich. Analytical reagent grade calcium chloride ($CaCl_2$), sodium carbonate (Na_2CO_3), absolute ethanol (CH_3CH_2OH), and all other reagents were purchased from Sinopharm Chemical Reagent Beijing Co. Ltd. The water used in all experiments was deionized water unless otherwise stated. All assays were performed in triplicate and data reported as average ± standard deviation.

Yeast Cell Preparations. *S. cerevisiae* YS58 yeast cells were kindly supplied by Dr. Junfeng Liu (Beijing University of Chemical Technology). Cells were grown batch-wise in medium (glucose 2.0%, peptone 2.0%, and pH 5.5) at 30 °C for 2 days with shaking at 180 rpm. The cells were collected, resuspended in 1/15 M phosphate buffer (pH 7.5), and used as a substrate for the determination of lytic activity.

Measurement of Lytic Activity of Zymolyase. An appropriate amount of enzyme (10 mg·mL^{-1}, 10 μL) was added to 200 μL of yeast suspension, and the change of absorbance at 620 nm was monitored. The reaction mixture was incubated at 25 °C for 2 h with gentle shaking. The turbidity of the reaction mixture and the number of intact cells in the mixture were determined after different time periods (t). Lysis of yeast cells was expressed as the percentage decrease in optical density (OD) at 620 nm and/or in cell number. In the control experiments, phosphate buffer was used instead of an enzyme solution, and clearing of cytoplasmic contents (cell wall lysis) because of autolysis was measured. The data of the free zymolyase was fitted to first-order rate kinetics to determine the apparent rate constant K_{cat}/K_m, where K_{cat} is the turnover number and K_m is the Michaelis constant. The activity of the immobilized zymolyase was assayed using the same method.

$$\text{Activity (percentage decrease in cell number)} = 1 - \frac{\text{Number of intact cells at time } t}{\text{Initial number of intact cells}} \quad (1)$$

$$\text{Substrate concentration } ([S]_t) = \frac{\text{Number of intact cells at time } t}{\text{mL}} \quad (2)$$

$$\text{Reaction rate } (v) = \frac{[S]_{initial} - [S]_t}{t} \quad (3)$$

$$v = \frac{V_{max}[S]}{K_m + [S]} \quad (4)$$

$$K_{cat} = \frac{V_{max}}{[E]} \quad (5)$$

$$\frac{1}{v} = \frac{K_m}{V_{max}}\frac{1}{[S]} + \frac{1}{V_{max}} \quad (6)$$

Preparation of Regenerated SF and SF-Based Hydrogels. Regenerated SF and chemically cross-linked SF-based hydrogels were prepared as previously described.[21−25] Briefly, raw silk (produced in Zhejiang, China) was degummed in 0.05 wt % Na_2CO_3 at 90 °C for 90 min and rinsed thoroughly with deionized water. The degummed silk was dissolved in a solution of $CaCl_2/CH_3CH_2OH/H_2O$ (with a molar ratio of 1:2:8) at 60 °C for 2 h and then collected by centrifuging at 8000 rpm for 12 min at 4 °C. The supernatant was dialyzed against deionized water using a cellulose dialysis membrane (MWCO 3500 Da) for 3 days and then lyophilized to obtain regenerated SF. SF (40 mg) was solubilized in 186 μL of PBS. APS (10 μL, 1 M) and $[Ru(bpy)_3]^{2+}Cl^-_2$ (4 μL, 20 mM) solutions were then added. The mixture was irradiated for 10 min using a 100 W fiber optical white light source placed 4 cm away. For zymolyase immobilization in the SF-based hydrogels, the procedure was the same except that SF was replaced with a mixture of SF and zymolyase.

Synthesis of Fe_3O_4 Magnetic Nanoparticles. The Fe_3O_4 nanoparticles were prepared by a coprecipitation

DOI: 10.1021/acsomega.9b03491
ACS Omega 2019, 4, 21612−21619

method.[32,33] An aqueous solution of $FeCl_3$ was mixed with a hydrochloric acid (HCl) solution of $FeCl_2$ at Fe^{3+}:Fe^{2+} = 2:1. To the mixture, the NaOH solution was added drop by drop with continuous stirring at 40 °C. When pH was adjusted to 10, a black precipitate appeared, which was kept for 30 min. The precipitate was washed three times with distilled water to remove excess NaOH and any impurity. The precipitate was further washed with ethanol and vacuum-dried (50 °C) for further use.

Preparation of Regenerated SF Microsphere-Embedded Fe_3O_4 Magnetic Nanoparticles. The vacuum-dried nanoparticles were redispersed in absolute ethanol. A certain amount of the above dispersion was added dropwise to 10% (w/w) RSF solutions (v/v = 3/20) under continuous gentle stirring at room temperature over 2 min. The mixture was incubated in a refrigerator at −20 °C for 24 h. Then, the frozen sample was defrosted. After centrifugation, followed by washing with water three times and by lyophilizing with a freezing dryer, stable microspheres (denoted as SF/Fe_3O_4) were separated using a magnet.[34,40]

Immobilization of Zymolyase on Regenerated SF Microsphere-Embedded Fe_3O_4 Magnetic Nanoparticles. The magnetic SF microspheres (1.8 mg) were dispersed in 164 μL of phosphate buffer solution (1/15 M, pH = 7.5) with dissolved 20 μL of zymolyase (10 mg·mL^{-1}). Following addition of APS (12 μL, 1 M) and $[Ru(bpy)_3]^{2+}Cl^-_2$ (4 μL, 20 mM), the solution was irradiated with white light. The resultant microspheres (denoted as ZY/SF/Fe_3O_4) were separated by magnetic separation and washed thoroughly with deionized water to remove remaining reagents, while the supernatant was kept to investigate the remaining content of zymolyase by the Bradford protein assay as previously described.[22] Immobilization efficiency (IE) was calculated by the following equation

$$\mathrm{IE} = 1 - \frac{\text{Remaining content of zymolyase in the supernatant}}{\text{Total content of zymolyase used in the immobilization}} \quad (7)$$

Amino Acid Analysis. Zymolyase was completely hydrolyzed in concentrated HNO_3 and used for amino acid analysis (Hitachi L-8900, Japan).

UV−Vis Spectroscopy. The absorbance was measured on a UV−vis spectrophotometer (Shimadzu UV-2600, Japan).

X-Ray Diffraction Analysis. Powder X-ray diffraction analysis (Shimadzu XRD-6000, Japan) was recorded in the range of 5−90° at a scan rate of 5° min^{-1} with CuK α radiation (λ = 0.15406 nm).

Thermal Gravimetric Analysis. TGA (TGA/DSC3, METTLER TOLEDO, USA) were measured under nitrogen atmosphere in a temperature range of 20−600 °C. The chemical composition was calculated according to the following equations

$$\text{Fe_3O_4 content in ZY/SF/Fe_3O_4}(\%) = 100\% - \text{weight loss in ZY/SF/Fe_3O_4}(\%) \quad (8)$$

$$\text{Fe_3O_4 content in SF/Fe_3O_4}\ (\%) = 100\% - \text{weight loss in SF/Fe_3O_4}\ (\%) \quad (9)$$

$$\text{SF content in SF/Fe_3O_4}\ (\%) = \text{weight loss in SF/Fe_3O_4}\ (\%) - \text{weight loss in Fe_3O_4}\ (\%) \quad (10)$$

Fourier Transform Infrared Spectroscopy. The FTIR spectra were obtained using an FTIR spectrometer (Bruker Optics VERTEX 70, USA) in the transmission mode in the range of 400−4000 cm^{-1} with a resolution of 4 cm^{-1} at room temperature.

Vibrating Sample Magnetometers. Magnetic properties were investigated by a vibrating sample magnetometer (VSM, BKT-4500, Beijing, China). The magnetic hysteresis curves were recorded at room temperature, in which the magnetism of materials could be characterized by parameters such as the saturation magnetization (M_s), the remanence (M_r), and the coercivity (H_c).

Dynamic Light Scattering. Particle size distribution was measured by DLS (Zetasizer Nano ZS90, Malvern Instruments, UK).

Scanning Electron Microscopy. The hydrogel samples were shock-frozen in liquid nitrogen and lyophilized. The obtained samples were fractured and coated with gold for SEM observation using a scanning electron microscope (Hitachi Regulus8100, Japan).

Transmission Electron Microscopy. For TEM experiments (Hitachi H-800, Japan), samples were dispersed in absolute ethanol and prepared by evaporating a droplet of the dispersion on a Cu grid.

■ ASSOCIATED CONTENT

Supporting Information

The Supporting Information is available free of charge at https://pubs.acs.org/doi/10.1021/acsomega.9b03491.

Detailed results on TGA, EDS and enzymolysis assays on the free and immobilized zymolyase (PDF)

■ AUTHOR INFORMATION

Corresponding Author

*E-mail: lvshanshan@mail.buct.edu.cn. Phone: (86)10-64411656. Fax: (86)10-64434784.

ORCID

Shanshan Lv: 0000-0002-6068-3048

Author Contributions

S.L. conceived the idea, designed the overall experiments, analyzed the data, and wrote the manuscript. M.X. designed, conducted, and analyzed the data of individual experiments and edited the manuscript. Both authors have given approval to the final version of the manuscript.

Notes

The authors declare no competing financial interest.

■ ACKNOWLEDGMENTS

The authors would like to thank Prof. Yan Zhang (Tianjin University) for helpful suggestion, Prof. Qiang Lyu (Soochow University) for kind assistance to buy raw silk, Yueying Han, Qinfu Lu, Haotian Yang, Li Han, Yanbing Feng, and Zihua Dong (Beijing University of Chemical Technology) for kind assistance on preparing regenerated silk fibroin and photochemically cross-linked silk fibroin-based hydrogels. This work was supported by the National Natural Science Foundation of

DOI: 10.1021/acsomega.9b03491
ACS Omega 2019, 4, 21612−21619

China (grant numbers: 21972009 and 31400813), the National Key Research Program of China (grant number: 2016YFA0201700/2016YFA0201701), and the Foundation of Beijing University of Chemical Technology (grant number: XK180301).

REFERENCES

(1) García-Saucedo, C.; Field, J. A.; Otero-Gonzalez, L.; Sierra-Álvarez, R. Low Toxicity of HfO_2, SiO_2, Al_2O_3 and CeO_2 Nanoparticles to the Yeast, Saccharomyces Cerevisiae. *J. Hazard. Mater.* **2011**, *192*, 1572−1579.
(2) Bystryak, S.; Santockyte, R.; Peshkovsky, A. S. Cell Disruption of S. Cerevisiae by Scalable High-Intensity Ultrasound. *Biochem. Eng. J.* **2015**, *99*, 99−106.
(3) Liu, D.; Lebovka, N. I.; Vorobiev, E. Impact of Electric Pulse Treatment on Selective Extraction of Intracellular Compounds from Saccharomyces Cerevisiae Yeasts. *Food Bioproc. Technol.* **2013**, *6*, 576−584.
(4) Liu, D.; Zeng, X. A.; Sun, D. W.; Han, Z. Disruption and Protein Release by Ultrasonication of Yeast cells. *Innov. Food Sci. Emerg.* **2013**, *18*, 132−137.
(5) Kitamura, K.; Kaneko, T.; Yamamoto, Y. Lysis of Viable Yeast Cells by Enzymes of Arthrobacter luteus. *Arch. Biochem. Biophys.* **1971**, *145*, 402−404.
(6) Hartmann, M.; Jung, D. Biocatalysis with Enzymes Immobilized on Mesoporous Hosts: the Status Quo and Future Trends. *J. Mater. Chem.* **2010**, *20*, 844−857.
(7) Stepankova, V.; Bidmanova, S.; Koudelakova, T.; Prokop, Z.; Chaloupkova, R.; Damborsky, J. Strategies for Stabilization of Enzymes in Organic Solvents. *ACS Catal.* **2013**, *3*, 2823−2836.
(8) Cipolatti, E. P.; Silva, M. J. A.; Klein, M.; Feddern, V.; Feltes, M. M. C.; Oliveira, J. V.; Ninow, J. L.; de Oliveira, D. Current Status and Trends in Enzymatic Nanoimmobilization. *J. Mol. Catal. B: Enzym.* **2014**, *99*, 56−67.
(9) DiCosimo, R.; McAuliffe, J.; Poulose, A. J.; Bohlmann, G. Industrial Use of Immobilized Enzymes. *Chem. Soc. Rev.* **2013**, *42*, 6437−6474.
(10) Sheldon, R. A.; van Pelt, S. Enzyme Immobilisation in Biocatalysis: Why, What and How. *Chem. Soc. Rev.* **2013**, *42*, 6223−6235.
(11) Rodrigues, R.; COrtiz, C.; Berenguer-Murcia, Á.; Torres, R.; Fernández-Lafuente, R. Modifying Enzyme Activity and Selectivity by Immobilization. *Chem. Soc. Rev.* **2013**, *42*, 6290−6307.
(12) Patel, S. K. S.; Choi, S. H.; Kang, Y. C.; Lee, J.-K. Eco-Friendly Composite of Fe_3O_4-Reduced Graphene Oxide Particles for Efficient Enzyme Immobilization. *ACS Appl. Mater. Interfaces* **2017**, *9*, 2213−2222.
(13) Liu, D. M.; Chen, J.; Shi, Y. P. Advances on Methods and Easy Separated Support Materials for Enzymes Immobilization. *TrAC, Trends Anal. Chem.* **2018**, *102*, 332−342.
(14) Mu, X.; Qiao, J.; Qi, L.; Dong, P.; Ma, H. Poly (2-vinyl-4, 4-dimethylazlactone)-Functionalized Magnetic Nanoparticles as Carriers for Enzyme Immobilization and Its Application. *ACS Appl. Mater. Interfaces* **2014**, *6*, 21346−21354.
(15) Wang, C.; Xu, H.; Liang, C.; Liu, Y.; Li, Z.; Yang, G.; Cheng, L.; Li, Y.; Liu, Z. Iron Oxide@ Polypyrrole Nanoparticles as a Multifunctional Drug Carrier for Remotely Controlled Cancer Therapy with Synergistic Antitumor Effect. *ACS Nano* **2013**, *7*, 6782−6795.
(16) Chen, Z.; Xu, W.; Jin, L.; Zha, J.; Tao, T.; Lin, Y.; Wang, Z. Synthesis of Amine-Functionalized Fe_3O_4@ C Nanoparticles for Lipase Immobilization. *J. Mater. Chem. A* **2014**, *2*, 18339−18344.
(17) Wang, X. Y.; Jiang, X. P.; Li, Y.; Zeng, S.; Zhang, Y. W. Preparation Fe_3O_4@ Chitosan Magnetic Particles for Covalent Immobilization of Lipase from Thermomyces Lanuginosus. *Int. J. Biol. Macromol.* **2015**, *75*, 44−50.
(18) Wang, S.; Xu, T.; Yang, Y.; Shao, Z. Colloidal Stability of Silk Fibroin Nanoparticles Coated with Cationic Polymer for Effective Drug Delivery. *ACS Appl. Mater. Interfaces* **2015**, *7*, 21254−21262.
(19) Lu, Q.; Wang, X.; Hu, X.; Cebe, P.; Omenetto, F.; Kaplan, D. L. Stabilization and Release of Enzymes from Silk Films. *Macromol. Biosci.* **2010**, *10*, 359−368.
(20) Kim, C. S.; Yang, Y. J.; Bahn, S. Y.; Cha, H. J. A Bioinspired Dual-Crosslinked Tough Silk Protein Hydrogel as a Protective Biocatalytic Matrix for Carbon Sequestration. *NPG Asia Mater.* **2017**, *9*, e391.
(21) Zhang, D.; Peng, H.; Sun, B.; Lyu, S. High Water Content Silk Protein-Based Hydrogels with Tunable Elasticity Fabricated via a Ru (II) Mediated Photochemical Cross-Linking Method. *Fibers Polym.* **2017**, *18*, 1831−1840.
(22) Han, Y.; Yu, S.; Liu, L.; Zhao, S.; Yang, T.; Yang, Y.; Fang, Y.; Lv, S. Silk Fibroin-Based Hydrogels as a Protective Matrix for Stabilization of Enzymes Against pH Denaturation. *Mol. Catal.* **2018**, *457*, 24−32.
(23) Li, S.; Chen, C.; Zhang, D.; Zhang, X.; Sun, B.; Lv, S. Microwave-Assisted Fast and Efficient Dissolution of Silkworm Silk for Constructing Fibroin-Based Biomaterials. *Chem. Eng. Sci.* **2018**, *189*, 286−295.
(24) Li, S.; Chen, C.; Zhang, Z.; Wang, D.; Lv, S. Illustration and Application of Enhancing Effect of Arginine on Interactions Between Nano-Clays: Self-Healing Hydrogels. *Soft Matter* **2019**, *15*, 303−311.
(25) Liu, L.; Han, Y.; Lv, S. Design of Self-Healing and Electrically Conductive Silk Fibroin-Based Hydrogels. *ACS Appl. Mater. Interfaces* **2019**, *11*, 20394−20403.
(26) Fei, X.; Shao, Z.; Chen, X. Hematite Nanostructures Synthesized by a Silk Fibroin-Assisted Hydrothermal Method. *J. Mater. Chem. B* **2013**, *1*, 213−220.
(27) Deng, M.; Huang, Z.; Zou, Y.; Yin, G.; Liu, J.; Gu, J. Fabrication and Neuron Cytocompatibility of Iron Oxide Nanoparticles Coated with Silk-Fibroin Peptides. *Colloid. Surface. B* **2014**, *116*, 465−471.
(28) Sheng, W.; Liu, J.; Liu, S.; Lu, Q.; Kaplan, D. L.; Zhu, H. One-Step Synthesis of Biocompatible Magnetite/Silk Fibroin Core−Shell Nanoparticles. *J. Mater. Chem. B* **2014**, *2*, 7394−7402.
(29) Tian, Y.; Jiang, X.; Chen, X.; Shao, Z.; Yang, W. Doxorubicin-Loaded Magnetic Silk Fibroin Nanoparticles for Targeted Therapy of Multidrug-Resistant Cancer. *Adv. Mater.* **2014**, *26*, 7393−7398.
(30) Samal, S. K.; Dash, M.; Shelyakova, T.; Declercq, H. A.; Uhlarz, M.; Bañobre-López, M.; Dubruel, P.; Cornelissen, M.; Herrmannsdörfer, T.; Rivas, J.; Padeletti, G.; de Smedt, S.; Braeckmans, K.; Kaplan, D. L.; Alek Dadiu, V. Biomimetic Magnetic Silk Scaffolds. *ACS Appl. Mater. Interfaces* **2015**, *7*, 6282−6292.
(31) Xie, X.; Luo, P.; Han, J.; Chen, T.; Wang, Y.; Cai, Y.; Liu, Q. Horseradish Peroxidase Immobilized on the Magnetic Composite Microspheres for High Catalytic Ability and Operational Stability. *Enzyme Microb. Technol.* **2019**, *122*, 26−35.
(32) Kang, Y. S.; Risbud, S.; Rabolt, J. F.; Stroeve, P. Synthesis and Characterization of Nanometer-Size Fe_3O_4 and γ-Fe_2O_3 Particles. *Chem. Mater.* **1996**, *8*, 2209−2211.
(33) Fried, T.; Shemer, G.; Markovich, G. Ordered Two-Dimensional Arrays of Ferrite Nanoparticles. *Adv. Mater.* **2001**, *13*, 1158−1161.
(34) Chen, X.; Shao, Z.; Knight, D. P.; Vollrath, F. Conformation Transition Kinetics of Bombyx Mori Silk Protein. *Proteins.* **2007**, *68*, 223−231.
(35) Li, Y.; Ding, M.; Wang, S.; Wang, R.; Wu, X.; Wen, T.; Yuan, L.; Dai, P.; Lin, Y.; Zhou, X. Preparation of Imprinted Polymers at Surface of Magnetic Nanoparticles for the Selective Extraction of Tadalafil from Medicines. *ACS Appl. Mater. Interfaces* **2011**, *3*, 3308−3315.
(36) Li, N.; Qi, L.; Shen, Y.; Qiao, J.; Chen, Y. Novel Oligo (ethylene glycol)-Based Molecularly Imprinted Magnetic Nanoparticles for Thermally Modulated Capture and Release of Lysozyme. *ACS Appl. Mater. Interfaces* **2014**, *6*, 17289−17295.

DOI: 10.1021/acsomega.9b03491
ACS Omega 2019, 4, 21612−21619

(37) Luo, X.; Zhang, L. Immobilization of Penicillin G Acylase in Epoxy-Activated Magnetic Cellulose Microspheres for Improvement of Biocatalytic Stability and Activities. *Biomacromolecules* **2010**, *11*, 2896−2903.
(38) Liu, Y.; Zeng, Z.; Zeng, G.; Tang, L.; Pang, Y.; Li, Z.; Liu, C.; Lei, X.; Wu, M.; Ren, P.; Liu, Z.; Chen, M.; Xie, G. Immobilization of Laccase on Magnetic Bimodal Mesoporous Carbon and the Application in the Removal of Phenolic Compounds. *Bioresour. Technol.* **2012**, *115*, 21−26.
(39) Patel, S. K. S.; Choi, S. H.; Kang, Y. C.; Lee, J.-K. Large-Scale Aerosol-Assisted Synthesis of Biofriendly Fe_2O_3 Yolk−Shell Particles: A Promising Support For Enzyme Immobilization. *Nanoscale* **2016**, *8*, 6728−6738.
(40) Cao, Z.; Chen, X.; Yao, J.; Huang, L.; Shao, Z. The Preparation of Regenerated Silk Fibroin Microspheres. *Soft Matter* **2007**, *3*, 910−915.

DOI: 10.1021/acsomega.9b03491
ACS Omega 2019, 4, 21612−21619